**Accredited Ranking SINTA 2**
Decree of the Director General of Higher Education, Research and Technology, No. 158/E/KPT/2021
Validity period from Volume 5 Number 2 of 2021 to Volume 10 Number 1 of 2026

Published online on: **http://jurnal.iaii.or.id**

**JURNAL RESTI**
**(Rekayasa Sistem dan Teknologi Informasi)**
Vol. 7 No. 3 (2023) 637 - 645 ISSN Media Electronic: 2580-0760

# Use of Plant Health Level Based on Random Forest Algorithm for Agricultural Drone Target Points

Try Kusuma Wardana[1], Yandra Arkeman[2], Karlisa Priandana[3], Farohaji Kurniawan[4]
[1,2,3]Computer Science Department, Faculty of Mathematics and Natural Sciences, Bogor Agricultural University (IPB)
[1,4]Aeronautics Technology Center, Research Organization for Aeronautics and Space, National Research and Innovation Agency (BRIN)
[1]trykusumawardana@apps.ipb.ac.id, [2]yandra@apps.ipb.ac.id, [3]karlisa@apps.ipb.ac.id, [4]farohaji.kurniawan@brin.go.id

***Abstract***

*Chemical residues from the use of pesticides in agriculture can impact human health through environmental and food pollution. To lessen the negative effects of excessive pesticide use, pesticides must be applied to plants by dose. The dose of pesticide application can be based on a plant health level, which is the result of drone Normalized Difference Vegetation Index (NDVI) image analysis. Drones can also be used for spraying pesticides. Analysis of plant health levels was carried out using the Random Forest (RF) algorithm. The results of the classification plant health levels will be used to design spray drone flight routes. The objective of this research is to classify plant health levels of rice based on NDVI imagery using the RF algorithm and to compile a database of spray drone target points. The results of this study indicate that the classification of plant health levels using the RF algorithm produces an accuracy value of 98% and a Kappa value of 0.96. As a result, the model developed and the algorithm employed is quite effective at classifying the level of plant health. Furthermore, spray drone target points based on plant health levels can be generated. Optimally the spray distance between rows is 2 m.*

*Keywords: NDV; drone; agriculture; random forest*

## 1. Introduction

Pesticides have been used in agriculture for more than two decades. Pesticides are important in agriculture because they can reduce plant disease and increase crop yields. Without pesticides, fruit production will decrease by 78%; vegetable production will decrease by 54%, and cereal production will decrease by 32% [1].

Chemical residues from the use of pesticides can impact human health through environmental and food pollution. In addition, climate change also impacts the increased use of pesticides that can cause pesticide pollution. When pesticides are used for plants or disposed of, they can experience movement and degradation so that they have the potential to pollute the environment [2], [3].

To reduce the negative impact of excessive use of pesticides, it is important to apply pesticides to plants according to the dose or dose. The dose of pesticides can be based on the health level of a plant. Monitoring the level of plant health can be done using drones. Drones with camera payloads can be used for plant health monitoring [4]–[6].

Monitoring plant health using drones produces image data to support accurate and reliable agricultural management. This image data can be generated from a multispectral camera mounted on a drone. Drone-mounted cameras produce more analytical and effective data compared to data from satellites [7]. In precision agriculture, decisions in crop management require accurate and reliable data with adequate spatial and temporal resolution. Therefore data generated from drones may be used instead of data from the Sentinel-2 satellite [8] as shown in figure 1 and 2.

In agriculture, apart from being used for crop monitoring, drones can also be used for spraying pesticides [6]. In general, the spraying of pesticides is still done manually (the operator brings the sprayer). The World Health Organization (WHO) states that many bad cases result from manually spraying plants [9]. However, most pesticide spraying (both manually and using drones) does not pay attention to the dose of pesticides given. The dose of pesticide application using drones can be based on the health level of a plant.

Accepted: 22-02-2023 | Received in revised: 15-04-2023 | Published: 02-06-2023

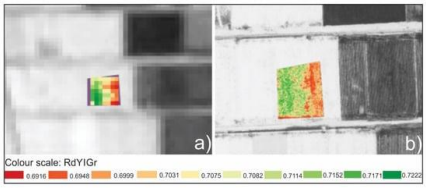


Figure 1. Comparison of image data (a) Sentinel-2 imagery, (b) Multispectral drone imagery with a scale of 1:1000 [7]

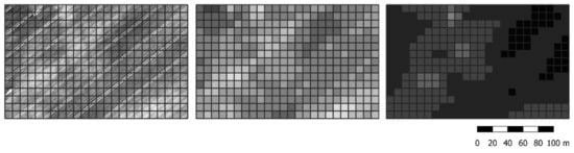


Figure 2. Near-infrared (NIR) image, Left: drone image resolution, Center: average drone image resolution, Right: sentinel image resolution [8]

Application of pesticides using spray drones requires analysis of flight routes. Spray drone flight routes can be adjusted to the level of plant health. Therefore the objective of this research is to classify plant health level based on NDVI imagery using the Random Forest (RF) algorithm, as well as create a database of point locations for spray drone operation targets that contain plant health level data. Plant health level data is processed using the RF algorithm because this algorithm has advantages, namely a high accuracy of classification results and the ability to measure variables important in mapping land cover areas. Indirectly, the benefits of this research are that it is hoped that pollution and environmental pollution due to the use of pesticides that are not following the dosage can be reduced, and it is hoped that farmers can be assisted in managing agricultural land properly and sustainably.

## 2. Research Methods

The ecosystem of the concept proposed in this study is that two types of drones have their respective functions as shown in figure 3. The first drone performs aerial mapping of the land area that will be used as an object. This mapping aims to produce images of agricultural land as material for analyzing plant health levels. The second drone functions to spray pesticides on plants. Spraying of pesticides is carried out based on the level of plant health (which may differ for each area of land). Spray drone flight routes are designed based on location points with plant health level parameters.

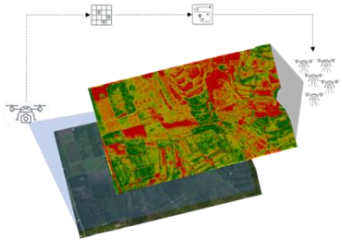

Figure 3. The general illustration of the ecosystem from the proposed concept

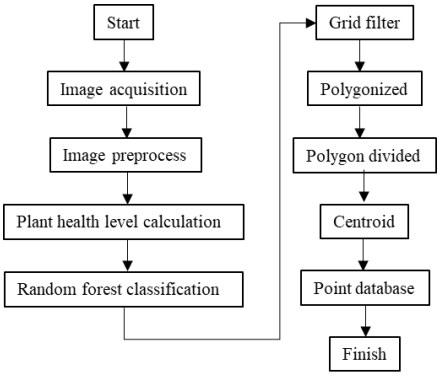


Figure 4. Flowchart of the stages of the research process

In general, the method in figure 4 is used to produce a database of agricultural drone target points based on plant health level data.

### 2.1 Mapping drones take land images

Drones used for land area mapping are equipped with multispectral camera payloads. The drone mapping used is a drone that has four propellers (quadcopter) with a diagonal size of 350 mm and a weight of 1478 grams. While the specifications of the camera used are as follows: sensors six 1/2.9" CMOS, effective pixels 2.08 MP (2.12 MP in total), field of view 62.7º, focal length 5.74 mm, and filter Blue (B): 45 nm±16 nm; Green (G): 560nm±16nm; Red(R): 650 nm±16 nm; Red-edge (RE): 730 nm±16 nm; Near-infrared (NIR) 840 nm±16 nm.

In taking land images as seen in figure 5, several flight settings are applied, including a flying altitude is 50 m, ground sampling distance or image resolution of about 3.1 cm/px, side lap is 75% and front lap is 75%.

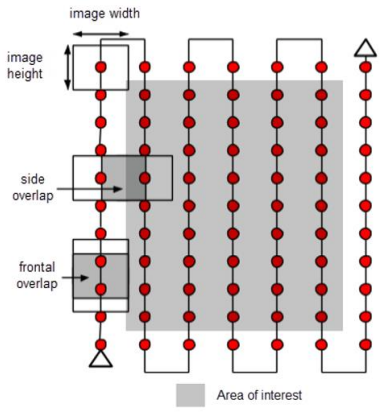


Figure 5. Illustration of drone flight settings for land imagery data acquisition

### 2.2 Pre-process image data (drone mapping results)

Land image data acquired using drone mapping, there are 5 image bands namely Red (R), Green (G), Blue (B), Near-infrared (NIR), and Red-Edge (RE) spectral

DOI: https://doi.org/10.29207/resti.v7i3.4959

bands. The process of combining images (mosaic) in each band is then carried out in the five types of images.

2.3 Plant health level

The level of plant health can be identified through the *vegetation index (VI)*. VI is a single value calculated by transforming observations from several spectral bands. Depending on the transformation method and the spectral band used, various aspects related to the vegetation cover in the image can be evaluated, for example, the percentage of vegetation cover, total chlorophyll content, leaf area index, and others. According to some experts, there are several approaches to see the level of plant health, including NDVI (Normalized Difference Vegetation Index), GNDVI (Green Normalized Difference Vegetation Index), EVI (Enhanced Vegetation Index), and SAVI (Soil Adjusted Vegetation Index) [10], [11].

Plant health levels are created to create certain classes based on attribute values (e.g., spectral values) of each image pixel. In this study, the NDVI approach was used to describe plant health. NDVI is a mathematical combination of the reflectance ratio between red band images and *near-infrared (NIR) band images*. In the NDVI data, the image spectral values range from 1 to -1. In general, the formula for NDVI can be written by formula 1 [10], [11]:

$$NDVI = \frac{NIR_{ref} - Red_{ref}}{NIR_{ref} - Red_{ref}} \quad (1)$$

where $NIR_{ref}$ is NIR spectral band value and $Red_{ref}$ is Red (R) spectral band value.

2.4 Random Forest Classification

The algorithm used to classify plant health levels is the Random Forest (RF) as seen in figure 6. Classification. RF has been developed and widely used for land cover classification [12]. RF is a machine-learning algorithm that can improve accuracy in terms of pattern recognition [13]. RF is based on a decision-tree algorithm with more than one decision tree [14]. Each training data calculates the most dominant class units to classify certain classes according to the input training data [15], [16].

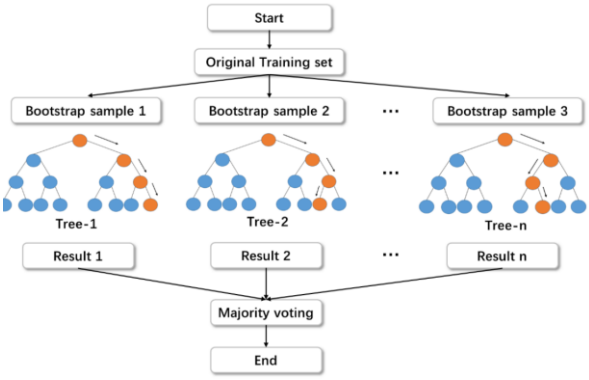


Figure 6. Stages of the Random Forest Algorithm process [17]

Information from drone image data is used to compile training data, which will then become input in the classification model. RGB images are used as reference or ground truth, while NDVI images are used as classification data. Process RF training and classification in this study was carried out with total data of 1134 pixels.

To measure the performance /accuracy of the classification model that has been made, a comparison of the actual value/ground truth value and the predicted value is carried out using the confusion matrix. A confusion matrix has been widely used to measure the performance of classification models in machine learning [18][19][20]–[22]. The accuracy test process will produce a value in which if the value is less than 80%, then it is necessary to re-create the training data to obtain a better classification model.

Besides overall accuracy, user accuracy and producer's accuracy are also calculated. User accuracy is related to the commission error, which is obtained by dividing the correct pixels in a class by the number of pixels in the class row, while producer accuracy is related to the commission error, which can be obtained by dividing the correct pixels in a class by the number of pixels in the class column. [18], [18], [23]. Respectively overall accuracy, user accuracy, producer's accuracy, and the Kappa coefficient can be calculated using formulas 2, 3, 4, 5, dan 6.

$$OA = \frac{(\sum_{i=1}^{r} X_{ii})}{N} \quad (2)$$

$$UA = \frac{X_{ii}}{X_{+1}} \quad (3)$$

$$PA = \frac{X_{ii}}{X_{1+}} \quad (4)$$

$$Kappa = \frac{OA - ECA}{1 - ECA} \quad (5)$$

Where:

DOI: https://doi.org/10.29207/resti.v7i3.4959

$$ECA = \sum_{i=1}^{r} Oe_i \times Ce_i \quad (6)$$

with $N$is total number of samples, $X_{ii}$ is the number of samples correctly classified in a category x, $X_{+1}$ is the number of samples of classification data in category x, $X_{1+}$ is number of samples from reference data in category x, $ECA$ is estimated chance agreement, $Oe_i$ is omission error in a category x and $Ce_i$ is commission error in a category x

2.5 Grid Filters

After the classification, the resulting image still has a few pixels that are different from the surrounding pixels. Therefore it is necessary to do a grid filter using the Majority Filter concept. The concept in figure 7 is to replace different pixel values with the same ones based on the majority value around them.

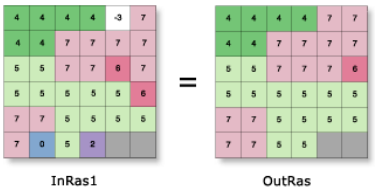


Figure 7. Majority Filter concept illustrations based on multiple pixel values

2.6 Polygonize

A polygonize process is carried out for further data analysis, which functions to convert raster data into vector data. Vector data in the form of polygons are created for all connected pixel areas in the raster that have pixel values The same. Each polygon vector is created with the attribute value of that pixel value.

2.7 Divided polygons

Function to divide vector polygon data with an area exceeding the specified area into several smaller polygons with the specified size. Each divided polygon has the same attributes as the previous polygon.

2.8 Centroids

To produce a point that matches the specified one, the midpoint data is needed from the polygon data resulting from the division. The midpoint attribute contains geometry data in the form of location data on the y-axis and x-axis as shown in figure 8.

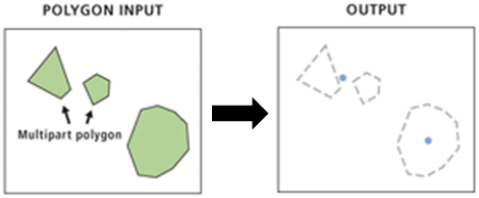


Figure 8. Illustration of center points of a polygon (one polygon area or 2 polygon areas)

2.9 Node with location data

The data set of points resulting from the centroid process contains geometry data in the form of longitude and latitude coordinate data and attributes in the form of plant health level data. These points will later be used to design spray drone flight routes.

## 3. Results and Discussions

3.1 Drone mapping takes land images

The land used as the research object is agricultural land with rice as a commodity. This land is located in Gobang Village, Rumpin District, Bogor Regency. There are several rice plants with different planting ages when the image data acquisition process is carried out on October 1, 2021.

From the data acquisition results, raw data is obtained from photo files consisting of the Red, Green, Blue, NIR, and RE bands. Each band consists of 317 photo files where the photo capture process follows predetermined flight settings (altitude, side lap, front lap). Each photo file in figure 9 overlaps with other photo files; this is because the overlap value that is applied is 75%. This overlap value is intended so that the resulting image is not perforated during the mosaic process.


Figure 9. Examples of raw image acquisition results are (a) RE band, (b) NIR band, (c) RGB band

DOI: https://doi.org/10.29207/resti.v7i3.4959

### 3.2 Pre-process drone mapping image data

The initial processing applied to the acquired image is the unification of all the raw data for each band. This process is known as the mosaic process can be seen in figure 10. The mosaic process is carried out based on the coordinate data contained in the metadata of the raw image file. This coordinate data is the location of the photo when the capture command is executed. The capture command will be executed when the drone is in a predetermined location or position. The data resulting from the mosaic process can be seen in Figure 10, where figure 10(a) is the result of the unification or mosaic of the raw RE band data, 10(b) is the result of the mosaic from the raw data of the NIR band, and 10(c) is the result of the mosaic of several bands namely the bands Red, Green, and Blue.

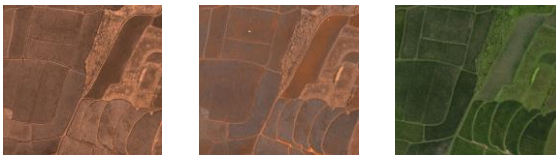

(a) (b) (c)

Figure 10. One part of the image resulting from the mosaic process, (a) RE band, (b) NIR band, (c) RGB band

### 3.3 Plant health level

Analysis of the health level of a plant is based on the vegetation index generated from drone imagery. The type of vegetation index used is the Normalized Difference Vegetation Index (NDVI) which represents the level of greenness (chlorophyll level) of a plant. NDVI image data has an attribute value for each image pixel. The pixel values are in the range -1 to 1, where a value of 1 can be interpreted as a plant with a high level of greenness representing a healthy plant condition, while -1 can be interpreted as a plant with a low greenness level which represents an unhealthy plant condition.

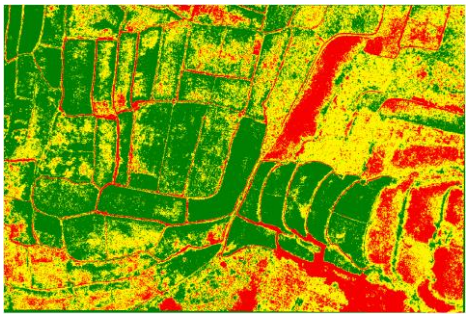

Figure 11. Image processing results using NDVI analysis

Figure 11 is the result of image data processing using NDVI analysis. The data is divided into 3 classes. Namely class 1 represents the condition of healthy plants (illustrated in green), class 2 represents the condition of unwell plants (illustrated in yellow), and class 3 represents the condition of unhealthy plants (illustrated in red).

Normalized Difference Vegetation Index spectral values and their meanings are shown in Table 1. This value representation is adopted from Marsujitullah (2023) [24].

Table 1. Representation of NDVI spectral values [24]

| Class | Spectral NDVI | Representation |
|---|---|---|
| Class 1 | -1.00 – 0.22 | Unhealthy |
| Class 2 | 0.23 – 0.39 | Unwell |
| Class 3 | 0.40 – 1.00 | Healthy |

### 3.4 Random Forest Classification

Classification is done by dividing the data into 3 classes: Healthy, Unwell, and Unhealthy, as classification data is NDVI image data resulting from drone mapping, while reference image data is high-resolution RGB image data. RGB image appearance data is used to validate the classification result data. The appearance of RGB images is more representative of the health level of plants; this is because the condition of plants is seen directly by humans through high-resolution images can be seen in figure 12. Visual interpretation will be very high due to using images with high resolution. Visual interpretation when using NDVI data in figure 13 will be difficult in the field because the spectrum of the Red and NIR bands cannot be seen directly by the human eye.

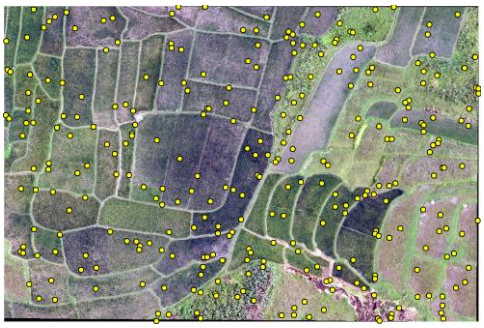

Figure 12. Sample points in modeling with RGB images as validation/reference data

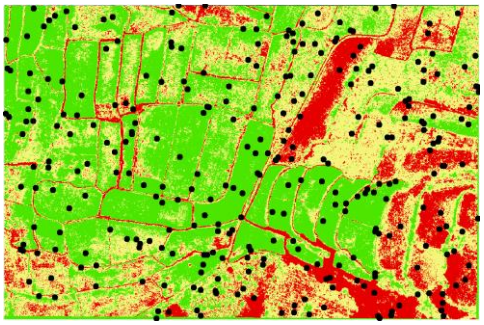

Figure 13. The sample points for testing the classification data are in the form of NDVI image data

Determining the area/point to be used as training data for the classification process is done by selecting several pixels most likely to match the NDVI image

DOI: https://doi.org/10.29207/resti.v7i3.4959

data (as test data) and their original appearance (as validation data). The appearance here is seen from several factors, including the leaves' condition and the plant's height. Pixel selection is determined randomly, in which all three classes must be represented in the selected pixels. In this study, 300 sample points were selected for training data.

Based on figure 14, the three classes will be classified using the RF algorithm. The first class is the unhealthy condition of the plants. It can be seen in Figure 14(a) that the pixel points in the NDVI image are red, so in the RGB image, they appear as areas/points that have sparse plants or damaged plant conditions. The second class is the condition of the plants being unwell. As shown in Figure 14(b) where the pixel points in the NDVI image are yellow, so in the RGB image, they appear as areas/points with a greater number of plants than the first class and a relatively green level of leaves. The third class is the condition of healthy plants. It can be seen in Figure 14(c) that the pixel points in the NDVI image are green, so in the RGB image, they appear as areas/points with a high plant density or a very good level of green leaves.

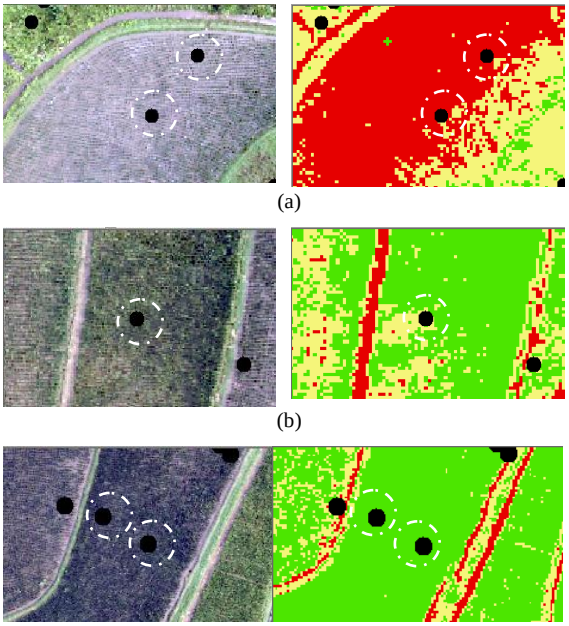

(a)

(b)

(c)

Figure 14. Comparison of plant conditions by visual appearance (RGB) and NDVI image data

Furthermore, the accuracy testing process is carried out to obtain the accuracy or performance of the classification method applied. Table 2 is the results of the accuracy test in the form of a confusion matrix. These values are the result of a comparison of the pixel values of the classified images with the pixel values of the reference images used as training data.

Table 2. Confusion matrix of classification results

| | | Classification | | | Total |
|---|---|---|---|---|---|
| | | Healthy | Unwell | Unhealthy | |
| Reference | Healthy | 120 | 6 | 0 | 126 |
| | Unwell | 2 | 118 | 1 | 121 |
| | Un-healthy | 0 | 1 | 52 | 53 |
| | Total | 122 | 125 | 53 | 300 |

Table 3. Calculation of producer and user accuracy

| Class | Producer's | | User's | |
|---|---|---|---|---|
| | Accuracy | Omission error | Accuracy | Commission errors |
| Healthy | 98% | 2% | 95% | 5% |
| Unwell | 94% | 6% | 97% | 3% |
| Unhealthy | 98% | 2% | 98% | 2% |

It can be seen in table 3 that 120 out of a total sample of 122 were classified as healthy plant condition classes with an omission error (misclassification in the healthy class) of 0.02%. In the unhealthy class column, classified as a healthy class of 6 samples and 1 sample of an unhealthy class, there is a commission error (additional classification from other classes) of 0.03%. The unhealthy plant condition class classified as another class is 1 sample, so there is a 2% commission error while the omission error is also 2%.

The overall accuracy value is calculated in formula 7.

$$OA = \frac{\text{Number of Correctly Classified Samples}}{\text{Number of Total Samples}} \quad (7)$$

$$OA = \frac{290}{300}$$

$$OA = 0.966667 = 96\%$$

While the following calculation obtains the Kappa value is in formula 8.

$$Kappa = \frac{OA - \text{Est.Chance Agreement}}{1 - \text{Est.Chance Agreement}} \quad (8)$$

$$Kappa = \frac{0.9667 - 0.002525}{1 - 0.002525}$$

$$Kappa = 0.966582$$

From the classification process, it is found that the overall accuracy value is 96%; this value shows good results from the classification process where the model created can be so accurate in classifying correctly. Some of the factors that cause this accuracy value include the similarity in visual appearance when carrying out the validation process. The validation process is carried out using high-resolution RGB image data; from these data, it can be seen that the greenness level of plants with adjacent classes (greenness levels between healthy class and unwell class, unwell class and unhealthy class) have similarities in the image data pixels.

DOI: https://doi.org/10.29207/resti.v7i3.4959

### 3.5 Grid Filtered

After the classification, the data can still not be analyzed because the resulting image still contains several pixels that are different from the surrounding pixels, commonly referred to as noise. In this case, the resulting image is divided into 3 classes: healthy, unwell, and unhealthy. For example, if there is still one healthy plant pixel in a pixel environment with a majority of unhealthy plant pixels, then that pixel will be generalized into a healthy plant pixel.

Several parameters must be set for image processing using the majority filter concept. One of the important parameters in the processing is the radius. The radius means the number of pixels used to generalize a reference pixel. Pixel generalization is carried out for pixels to the left, right, top, and bottom of a reference pixel. Figure 15 shows the difference between the original image/before and after the majority filter process.

From the Majority Filter process, by varying several radii, what will be used is the resulting MF image with 5 radii. Regarding the resulting image, which has a pixel size of 20 x 20 cm, if 5 radii are used in the MF process, an image with a minimum area size of 2 x 2 meters will be produced. This is based on several factors, the first is the flying height of the sprayer drone. Referring to the experience that has been done, the drone sprayer will optimally fly at a height of about 3 meters above the ground. In flight, the drone sprayer will cause strong wind gusts down or toward the plants. Therefore, flying at a height of 3 meters will be sufficient and optimal. Second is the nozzle's ability to spray. The spray power of a drone sprayer depends on the number of nozzles, pump specifications, and the power used. In general, sprayer drones that fly at a height of 3 meters, pesticide liquid will reach or hit plants at a radius of about 2 meters.

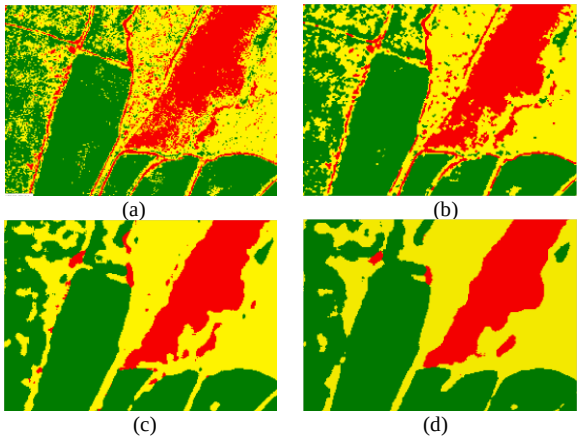


Figure 15. Comparison of images before and after the Majority Filter (MF) process, (a) Original image / before MF, (b) MF 1 radius, (c) MF 3 radius, and (d) MF 5 radius.

From the majority process that has been carried out, the result is that the total area used as the data set is 28039.19895 $m^2$, divided into 3 areas can be seen in figure 16 based on the level of plant health . The area with healthy plant conditions is 12270.252 $m^2$ or 44%, the area with unwell plant conditions is 12256.53 $m^2$ or 44%, and the area with unhealthy plant conditions is 3512.417 $m^2$ or 13%.

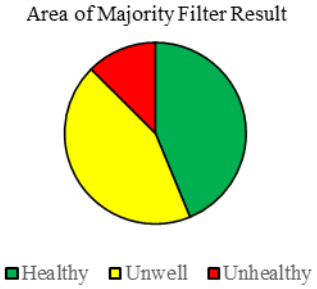


Figure 16. Areas based on the level of plant health after the majority filter process

### 3.6 Polygonize

Next, the Polygonize process is carried out, which converts raster data into vector data to be analyzed later. The created polygon area refers to the attribute values of the previous raster data. If the attribute value of a pixel area is healthy plants, then that area will be used as one polygon area of healthy plants.

### 3.7 Divided Polygon

Polygon divide in figure 17 is used to divide a very large polygon area (more than the size of a predetermined area) into small areas according to what has been determined. One of the parameters used to divide the polygon area is the size of the polygon area. In determining the size of small polygon areas, there are several factors, namely the height of the drone flying and the drone's ability to spray. These factors are the same when determining the radius value in the Majority Filter process. The large polygon area will be divided into polygon areas of 2 x 2 meters.

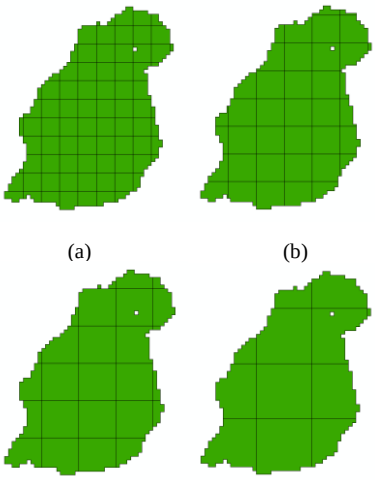


DOI: https://doi.org/10.29207/resti.v7i3.4959

(c) (d)

Figure 17. Splitting the polygon area into areas with predetermined sizes, (a) Grid 1x1, (b) Grid 1.5x1.5, (c) Grid 2x2, (d) Grid 3x3

### 3.8 Centroid and location point with geometry data

Searching for centroids or geometry center points is done to find out or find the midpoints of small polygon areas. The optimal distance of these points is 2 m (adjusting the data from the small polygons made). These location points will later be used as targets for spray drones. In these points, there are attribute data in the form of plant health conditions (healthy, unwell, or unhealthy) and location coordinates (longitude and latitude) can be seen in Figure 18 and table 4.

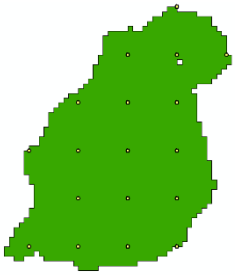

Figure 18. Visualization of the placement of spray drone target points along with point data attributes in the form of coordinate data (longitude and latitude)

Table 4. The form of coordinate data (longitude and latitude)

| Longitude | Latitudes |
|---|---|
| 106.6466 | -6.50793 |
| 106.6465 | -6.50795 |
| 106.6466 | -6.50795 |
| 106.6466 | -6.50795 |
| 106.6465 | -6.50797 |
| 106.6465 | -6.50797 |
| 106.6466 | -6.50797 |
| 106.6465 | -6.50799 |
| 106.6465 | -6.50799 |
| 106.6465 | -6.50799 |
| 106.6466 | -6.50799 |
| 106.6465 | -6,508 |
| 106.6465 | -6,508 |
| 106.6466 | -6,508 |
| 106.6465 | -6.50802 |
| 106.6465 | -6.50802 |
| 106.6465 | -6.50802 |
| 106.6466 | -6.50802 |

## 4. Conclusion

The topic discussed in this study is the use of random forest algorithm-based plant health data to create target points for spray drones. The plant health level (with rice as a comodity in this research) results from the image analysis from a multispectral camera attached to the drone. There are 5 bands of image data, namely red, green, blue, NIR, and RE bands. Plant health level analysis was carried out using Red and NIR band imagery through the NDVI approach. NDVI values are in the range -1 to 1, where -1 to 0.22 represents unhealthy plant conditions (illustrated in red), 0.23 to 0.39 represents unwell plant conditions (illustrated in yellow), and 0.40 to 1 represents healthy plant conditions (illustrated in green).

The plant health level data is then classified using the random forest (RF) algorithm, divided into 3 classes: healthy, unwell, and unhealthy. Red, green, and blue (RGB) image data is used for validation or ground truth, while NDVI imagery is used for classification data. The use of high-resolution RGB imagery because the condition of the plants can be seen directly by the human eye. The points used as training data were determined randomly from as many as 300 sample points. From the classification process, an accuracy value of 96% is obtained, and a Kappa value is 0.96. This value shows pretty good results, where the model can accurately classify it correctly. Similar studies were conducted by Svoboda et al with 89.1% accuracy dan Kappa 0.84 [25], Yuhao, et al with 89% accuracy and Kappa 0.81 [26], and Marlina with 91.39% accuracy dan Kappa 0.88 [27]. Some of the factors that cause this accuracy value include the similarity in visual appearance when carrying out the validation process. The validation process is carried out using high-resolution RGB image data. From these data, it can be seen that the greenness level of plants with adjacent classes (greenness levels between the healthy class and unwell class, unwell class and unhealthy class) have similarities in the image data pixels.

In addition to plant health level data, this research also succeeded in creating a database of location points based on a plant health level. The optimal distance between spray drone target points is 2 meters. Several factors are used in determining the distance between points, namely the flying height of the spraying drone and the ability of the nozzle to spray.

## Acknowledgment

This research is supported in part by Drone Precision Farming. The authors would like to thank the financial support provided by the Indonesia Research and Innovation Agency (BRIN) through the Degree by Research (DBR) scholarship. The authors would like to give their gratitude to all parties involved in supporting this research.

## References

[1] M. Tudi *et al.*, "Agriculture development, pesticide application and its impact on the environment," *International Journal of Environmental Research and Public Health*, vol. 18, no. 3. MDPI AG, pp. 1–24, 01-Feb-2021, doi: 10.3390/ijerph18031112.

[2] M. T. Scholtz and T. F. Bidleman, "Modelling of the long-term fate of pesticide residues in agricultural soils and their surface exchange with the atmosphere: Part II. Projected long-term fate of pesticide residues," *Sci. Total Environ.*, vol. 377, no. 1, pp. 61–80, May 2007, doi:

10.1016/J.SCITOTENV.2007.01.084.

[3] Y. Liu, R. Mo, F. Tang, Y. Fu, and Y. Guo, "Influence of different formulations on chlorpyrifos behavior and risk assessment in bamboo forest of China," *Environ. Sci. Pollut. Res. 2015 2224*, vol. 22, no. 24, pp. 20245–20254, Aug. 2015, doi: 10.1007/S11356-015-5272-2.

[4] M. Reinecke and T. Prinsloo, "The influence of drone monitoring on crop health and harvest size," *2017 1st Int. Conf. Next Gener. Comput. Appl. NextComp 2017*, pp. 5–10, Aug. 2017, doi: 10.1109/NEXTCOMP.2017.8016168.

[5] K. Neupane and F. Baysal-Gurel, "Automatic Identification and Monitoring of Plant Diseases Using Unmanned Aerial Vehicles: A Review," *Remote Sens. 2021, Vol. 13, Page 3841*, vol. 13, no. 19, p. 3841, Sep. 2021, doi: 10.3390/RS13193841.

[6] A. Hafeez *et al.*, "Implementation of drone technology for farm monitoring & pesticide spraying: A review," *Inf. Process. Agric.*, Feb. 2022, doi: 10.1016/J.INPA.2022.02.002.

[7] N. Bollas, E. Kokinou, and V. Polychronos, "Comparison of sentinel-2 and uav multispectral data for use in precision agriculture: An application from northern greece," *Drones*, vol. 5, no. 2, 2021, doi: 10.3390/drones5020035.

[8] J. Bukowiecki, T. Rose, and H. Kage, "Sentinel-2 data for precision agriculture?—a uav-based assessment," *Sensors*, vol. 21, no. 8, Apr. 2021, doi: 10.3390/s21082861.

[9] U. R. Mogili and B. B. V. L. Deepak, "Review on Application of Drone Systems in Precision Agriculture," *Procedia Comput. Sci.*, vol. 133, pp. 502–509, Jan. 2018, doi: 10.1016/J.PROCS.2018.07.063.

[10] D. Fawcett *et al.*, "Multi-Scale Evaluation of Drone-Based Multispectral Surface Reflectance and Vegetation Indices in Operational Conditions," *Remote Sens. 2020, Vol. 12, Page 514*, vol. 12, no. 3, p. 514, Feb. 2020, doi: 10.3390/RS12030514.

[11] R. Houborg and M. F. McCabe, "High-Resolution NDVI from Planet's Constellation of Earth Observing Nano-Satellites: A New Data Source for Precision Agriculture," *Remote Sens. 2016, Vol. 8, Page 768*, vol. 8, no. 9, p. 768, Sep. 2016, doi: 10.3390/RS8090768.

[12] C. Diniz *et al.*, "Brazilian Mangrove Status: Three Decades of Satellite Data Analysis," *Remote Sens. 2019, Vol. 11, Page 808*, vol. 11, no. 7, p. 808, Apr. 2019, doi: 10.3390/RS11070808.

[13] L. Breiman, "Random forests," *Mach. Learn.*, vol. 45, no. 1, pp. 5–32, Oct. 2001, doi: 10.1023/A:1010933404324/METRICS.

[14] I. Jamaluddin, Y.-N. Chen, S. M. Ridha, P. Mahyatar, and A. G. Ayudyanti, "Two Decades Mangroves Loss Monitoring Using Random Forest and Landsat Data in East Luwu, Indonesia (2000–2020)," *Geomatics 2022, Vol. 2, Pages 282-296*, vol. 2, no. 3, pp. 282–296, Jul. 2022, doi: 10.3390/GEOMATICS2030016.

[15] A. D. Kulkarni and B. Lowe, "Random Forest Algorithm for Land Cover Classification International Journal on Recent and Innovation Trends in Computing and Communication Random Forest Algorithm for Land Cover Classification," *Int. J. Recent Innov. Trends Comput. Commun.*, 2016.

[16] T. Noi Phan, V. Kuch, and L. W. Lehnert, "Land Cover Classification using Google Earth Engine and Random Forest Classifier—The Role of Image Composition," *Remote Sens. 2020, Vol. 12, Page 2411*, vol. 12, no. 15, p. 2411, Jul. 2020, doi: 10.3390/RS12152411.

[17] K. Guo, X. Wan, L. Liu, Z. Gao, and M. Yang, "Fault Diagnosis of Intelligent Production Line Based on Digital Twin and Improved Random Forest," *Appl. Sci. 2021, Vol. 11, Page 7733*, vol. 11, no. 16, p. 7733, Aug. 2021, doi: 10.3390/APP11167733.

[18] A. E. Maxwell and T. A. Warner, "Thematic Classification Accuracy Assessment with Inherently Uncertain Boundaries: An Argument for Center-Weighted Accuracy Assessment Metrics," *Remote Sens. 2020, Vol. 12, Page 1905*, vol. 12, no. 12, p. 1905, Jun. 2020, doi: 10.3390/RS12121905.

[19] X. Xu, H. Yuan, M. Liptrott, and M. Trovati, "Two phase heuristic algorithm for the multiple-travelling salesman problem," *Soft Comput.*, vol. 22, no. 19, pp. 6567–6581, Oct. 2018, doi: 10.1007/S00500-017-2705-5/TABLES/5.

[20] A. E. Maxwell, T. A. Warner, and L. A. Guillén, "Accuracy Assessment in Convolutional Neural Network-Based Deep Learning Remote Sensing Studies—Part 1: Literature Review," *Remote Sens. 2021, Vol. 13, Page 2450*, vol. 13, no. 13, p. 2450, Jun. 2021, doi: 10.3390/RS13132450.

[21] A. E. Maxwell, T. A. Warner, and L. A. Guillén, "Accuracy Assessment in Convolutional Neural Network-Based Deep Learning Remote Sensing Studies—Part 2: Recommendations and Best Practices," *Remote Sens. 2021, Vol. 13, Page 2591*, vol. 13, no. 13, p. 2591, Jul. 2021, doi: 10.3390/RS13132591.

[22] I. L. Sari, C. J. Weston, G. J. Newnham, and L. Volkova, "Assessing Accuracy of Land Cover Change Maps Derived from Automated Digital Processing and Visual Interpretation in Tropical Forests in Indonesia," *Remote Sens. 2021, Vol. 13, Page 1446*, vol. 13, no. 8, p. 1446, Apr. 2021, doi: 10.3390/RS13081446.

[23] S. S. Rwanga, J. M. Ndambuki, S. S. Rwanga, and J. M. Ndambuki, "Accuracy Assessment of Land Use/Land Cover Classification Using Remote Sensing and GIS," *Int. J. Geosci.*, vol. 8, no. 4, pp. 611–622, Apr. 2017, doi: 10.4236/IJG.2017.84033.

[24] Marsujitullah, D. A. Kaligis, and F. X. Manggau, "Health Analysis Of Rice Plants Based On The Normalized Difference Vegetation Index (Ndvi) Value In Image Of Unmanned Aircraft (Case Study Of Merauke - Papua Selatan)," *Eng. Technol. J.*, vol. 08, pp. 1986–1991, Feb. 2023, doi: 10.5281/ZENODO.7648523.

[25] J. Svoboda, P. Štych, J. Laštovička, D. Paluba, and N. Kobliuk, "Random Forest Classification of Land Use, Land-Use Change and Forestry (LULUCF) Using Sentinel-2 Data—A Case Study of Czechia," *Remote Sens. 2022, Vol. 14, Page 1189*, vol. 14, no. 5, p. 1189, Feb. 2022, doi: 10.3390/RS14051189.

[26] Y. Jin, X. Liu, Y. Chen, and X. Liang, "Land-cover mapping using Random Forest classification and incorporating NDVI time-series and texture: a case study of central Shandong," *https://doi.org/10.1080/01431161.2018.1490976*, vol. 39, no. 23, pp. 8703–8723, Dec. 2018, doi: 10.1080/01431161.2018.1490976.

[27] D. Marlina, "Klasifikasi Tutupan Lahan pada Citra Sentinel-2 Kabupaten Kuningan dengan NDVI dan Algoritme Random Forest," *STRING (Satuan Tulisan Ris. dan Inov. Teknol.*, vol. 7, no. 1, pp. 41–49, Aug. 2022, doi: 10.30998/STRING.V7I1.12948.

DOI: https://doi.org/10.29207/resti.v7i3.4959